Interannual variations of river water storage from a multisatellite approach: a case study for the Rio Negro River basin

Frédéric Frappart, Fabrice Papa, James S. Famiglietti, Catherine Prigent, William B. Rossow, F. Seyler

Interannual Variations of River Water Storage from a Multiple Satellite Approach: A case study for the Rio Negro River basin

Frédéric Frappart [1,*], Fabrice Papa [2], James S. Famiglietti [1], Catherine Prigent [3], William B. Rossow [2], Frédérique Seyler [4]

Submitted to Journal of Geophysical Research Atmospheres, September 2007.

Affiliations:

(1) Department of Earth System Science, University of California, Irvine, USA.

(2) NOAA-Cooperative Remote Sensing Science and Technology Center, City College of New York, New York, USA.

(3) CNRS, Laboratoire d'Etudes du Rayonnement et de la Matiere en Astrophysique, Observatoire de Paris, France.

(4) IRD, Brasilia, Brazil

(∗) Now at CESBIO, 14 Avenue Edouard Belin, 31400 Toulouse, France.

Corresponding author: frederic.frappart@cesbio.cnes.fr

Abstract:

Spatio-temporal variations of water volume over inundated areas located in a large river basin have been determined using combined observations from a multi-satellite inundation dataset, the Topex/Poseidon (T/P) altimetry satellite, and *in situ* hydrographic stations for the water levels over rivers and floodplains. We computed maps of monthly surface water volume change over the period of common availability of T/P and the multisatellite data (1993-2000). The basin of the Negro River, the largest tributary in terms of discharge to the Amazon River, was selected as a test site. A strong seasonal signal is observed with minima in October and maxima in June. A strong interannual component is also present, particularly important during ENSO years. The surface water change was estimated to be 167 ± 39 km^3 between October 1995 (low water) and June 1996 (high water). This result is consistent with previous estimates obtained for the 1995-1996 hydrological cycle over the same area using the JERS mosaic data. The surface water volume change is then compared to the total water volume change inferred from the GRACE satellite for an average annual cycle. The total water storage for the Negro River basin is almost equally partitioned between surface water and the combination of soil moisture and groundwater.

The water volume changes are also evaluated using in-situ discharge measurements and the GPCP precipitation product (correlation of 0.61). The results show the high potential for the new technique to provide valuable information to improve our understanding of large river basin hydrologic processes.

I. INTRODUCTION AND BACKGROUND

Terrestrial waters represent less than 1 % of the total amount of water on Earth. However, they have crucial impact on terrestrial life and human needs, and play a major role in climate variability [*Cosandey and Robinson*, 2000; *Perrier and Tuzet*, 2005]. Among the various reservoirs in which fresh water on land is stored (ice caps, glaciers, snow pack, soil moisture, groundwater, etc.), surface waters (rivers, lakes, reservoirs, wetlands and inundated areas) play a crucial role in the global biochemical and the hydrological cycles [*de Marsily et al*., 2005]. Even if wetlands and floodplains cover about 6 % of the Earth surface [*OECD*, 1996], they have a substantial impact on flood flow alteration, sediment stabilization, water quality, groundwater recharge and discharge [*Maltby*, 1991; *Bullock and Acreman*, 2003]. Variations in the extent of inundated surfaces and wetlands also contribute to the interannual variability of methane surface emissions [*Richey et al.*, 2002; *Bousquet et al.*, 2006]. Moreover, floodplain inundation is an important regulator of river hydrology owing to storage effects along channel reaches. Extensive floodplains along large South American rivers, such as Amazon, Paraná or Orinoco, have a significant role in the hydrological cycle of fluvial basins. Transport of water and sediments by rivers is substantially modified during residence of river water in floodplains. During its stay in these inundation areas, river water from is not only delayed in its transit to sea and affected by evapotranspiration, but it is also often subject to large biogeochemical changes due to sedimentation, nutrient uptake by the biota, and modifications of redox conditions [*Hamilton et al.*, 2002]. The water storage in these wetlands and its outflow represent a significant part of the water balance in the basin [*Richey et al.*, 1989; *Alsdorf et al.*, 2001].

Analysis of the flow and storage of fresh water over land is thus a key issue for understanding the terrestrial branch of the global water cycle, and is now recognized to have major importance for climate research as well as for inventory and management of water resources [*Bullock and Acreman*, 2003]. However, given that a large number of the world floodplains and wetlands are only inundated during some portion of the year, our current knowledge of the inter-seasonal and inter-annual variability of the land surface water storage cycle at the regional to global scales is still rather incomplete [*Matthews*, 2000].

Quantifying temporal variations in water volume stored in river floodplains has many practical applications, and further, would help improve understanding of the controlling mechanisms, inundation extent and their influence on the river water budget. For inundated areas permanently or temporarily connected to main channels, determining water volume variations is equivalent to estimating the potential water volume stored and/or released by a valley reach during flood stage. These water volume variations are an important variable for hydrodynamic modeling of river flow and the determination of river transport capacity. For inundated areas that never connect to the main channel, volume variations are essentially a function of baseflow variations, inputs from the local basin and rainfall. In all cases, the inundated area is a buffer zone between the river and the upland watershed, and its water volume variation represents the flood pulse of floodplains as expressed by *Junk et al.,* [1989]. It is also a key biogeochemical and ecological characteristic, which unfortunately, cannot be easily measured in the field [*Alsdorf and Lettenmaier*, 2003].

Until recently, estimates of floodplain volume variations within large river basins have essentially relied on hydrological models [*Coe et al.*, 2002; *Winsemius et al*. 2006]. *In situ* gauge measurements have helped to quantify the movement of water (discharge, height) in river channels, but provide comparatively little information about the spatial dynamics, height variations and volume storage of surface water, within floodplains and wetlands. In addition, some regions are completely ungauged and the number of ground-based stations has dramatically decreased during the last decade [*Alsdorf and Lettenmaier*, 2003]. Lacking spatial measurements of surface water volumetric changes, hydrological models are unable to properly represent the effects of surface storage on river discharge [Alsdorf, 2003; Alsdorf et al., 2007].

In recent years, remote sensing techniques have clearly shown the capability to monitor components of the water balance in large river basins [*Famiglietti*, 2004]. They are particularly very useful to surface water hydrology investigations [*Smith,* 1997, *Alsdorf et al.*, 2007] as they provide a unique mean to observe continuously large regions and are the only alternative to the lack of *in situ* data in remote areas. For example, satellite altimetry has been used for systematic monitoring of water levels of large rivers, lakes and floodplains (e.g., *Birkett*, 1998; *Mercier et al.*, 2002; *Maheu et al*., 2003). Synthetic Aperture Radar (SAR) Interferometry [*Alsdorf et al.*, 2000; *Alsdorf et al.*, 2001; and passive and active microwave observations [*Sippel et al*., 1998] also give crucial information on land surface water dynamics. Recently, the development of a multi-satellite technique to estimate water surface extent shows great potential; for example, *Prigent et al*. [2007] now offers the first global estimates of monthly inundation extents over most of a decade (1993-2000) and at a 0.25° horizontal resolution. In addition, new

space gravity missions, such as the GRACE mission, offer for the first time the possibility of directly measuring the spatio-temporal variations of total terrestrial water storage [*Wahr et al*., 2004; *Tapley et al*., 2004b; *Chen et al*., 2005a,b; *Ramillien et al.*, 2005; *Seo et al.*, 2006; *Lettenmaier and Famiglietti*, 2006; *Syed et al.*, 2007].

Frappart et al. [2005, 2006a] estimate water storage changes using remote sensing by combining high resolution imagery-derived inundation extents and altimetry-derived water level measurements in the Negro River and Mekong basins respectively. The technique showed encouraging results, but suffered from a lack of temporal coverage, as the SAR data from JERS are only available for two months in 1995-1996. In this paper, we propose a new approach to estimate river volume changes in a large drainage basin that combines estimates of spatial and temporal surface water extent from a multi-satellite technique [*Prigent et al.*, 2007] with water level measurements from satellite altimetry. The method is developed and presented as a case study over the Negro river in the Amazon basin. The results of this study will improve our understanding of large river basin hydrologic processes and modeling.

II. THE STUDY REGION

The Negro River sub-basin (700,000 km^2, Fig. 1) occupies 12% of the Amazon basin. It is the largest tributary to the Amazon River and ranks as the fifth largest river in the world for its water discharge [*Meade et al.*, 1991; *Molinier et al.*, 1995]. The Negro joins the Solimões River to form the Amazon River downstream from Manaus, and drains about 700,000 km² of Colombia (10%), Venezuela (6%), Guyana (2%) and Brazil (82%). It extends from 73.25° to 59.35° longitude West and from 5.4° North to 3.35° latitude

South. It is characterized by the dark color of its water, due to high content in dissolved organic matter and a low sediment load [*Sternberg*, 1975], and is a low gradient river, which partly accounts for the considerable extent of the floodplains (along with the large amount of precipitation). Rainfall in the sub-basin varies greatly both in space and time. Mean annual precipitation rates vary by more than 50% within the Negro river basin, from less than 2000 mm/yr (minimum values less than 1700 mm/yr are recorded in the northern part of the Branco River basin), to between 2250 and 2500 mm/yr near Manaus and up to 3000 mm/yr in the northwest [*Liebmann and Marengo*, 2001]. The timing of the rainy season differs widely along a south to north gradient: the beginning of the rainy season occurs in December in the south and in March or April in the north, whereas the rainy period ends from May to October [*Marengo et al.*, 2001].

III. DATASETS

A. Multi-satellite-derived inundation dataset

The methodology developed to quantify the extent and seasonality of land surface inundation at the global scale with a suite of satellites is described in detail in Prigent et al. [2001a; 2001b; 2007]. The satellite observations used to derive the inundation dataset cover a large portion of the electromagnetic spectrum:

1) passive microwave emissivities at 37 GHz (0.81 cm), estimated from SSM/I by removing the contributions of the atmosphere (water vapor, clouds, rain) and the modulation by the surface temperature, using ancillary data from visible and infra-red satellite observations from the International Satellite Cloud Climatology Project (ISCCP)

[*Rossow and Schiffer*, 1999] and the National Center for Environment Prediction (NCEP) reanalysis [*Kalnay et al*, 1996]. The emissivity calculation is detailed in *Prigent et al*. [2006].

2) ERS active microwave instrument backscattering coefficients at 5.25 GHz (5.71 cm).

3) AVHRR visible (0.58 − 0.68μm) and near-infrared (0.73−1.1μm) reflectances and derived NDVI, from the NDVI AVHRR 8 km product, generated under the joint NASA and NOAA Earth Observing System Pathfinder project [*James and Kalluri*, 1994],

A full description of each satellite observation and the potential of merged satellite data to study inundated surfaces can be found in *Prigent et al.*, [2001b].

The method to estimate surface water extent is a three-step process. First, each satellite data set is pre-processed. All the satellite observations are mapped onto an equal area grid of $0.25^{o}\times0.25^{o}$ resolution at the equator, chosen for consistency with global climate studies and compatibility with the other satellite spatial resolutions.

Second, an unsupervised clustering algorithm is used to merge the three sets of satellite observations. This algorithm has already shown the potential to characterize large-scale features of the density and seasonality of vegetation [*Prigent et al.*, 2001b] and it is refined for surface water detection. A sensitivity analysis has been conducted to select an optimal subset of observations that are used as input to the clustering scheme for water surface detection. Examination of the resulting cluster maps enables the selection of the classes that are related to inundated areas [*Prigent et al*., 2001a].

The last step consists of quantifying the fractional inundation extent within each pixel previously classified as inundated. Detection of inundation primarily relies on the passive microwave land-surface signal from SSM/I. Inundated regions are characterized by a

decrease of microwave emissivities and an increase of the emissivity polarization difference, even under dense canopy conditions. Because the ERS scatterometer shows minimal response to the presence of inundation, but is very sensitive to vegetation density [*Prigent et al.*, 2001 b], it is used to assess vegetation contributions to the passive microwave observations. A linear mixture model that relies on the statistical relationship between polarization differences in emissivities and backscatter is used to quantify inundated area.

Global monthly-mean maps of inundation extent are created with a $0.25^{o}\times0.25^{o}$ spatial resolution at the equator. The technique is globally applicable without any tuning for individual environments [*Prigent et al*., 2007]. Case studies for specific regions and environments are presented for India by *Papa et al*. [2006b],for the Ob river basin in *Papa et al*. [2007a] and for the large Siberian Watersheds in *Papa et al*. [2007b]. This dataset has been also recently used for hydrologic and climatic analyses, such as the evaluation of the methane surface emissions models [*Bousquet et al.*, 2006], the validation of river flooding scheme performances in land surface models [*Decharme et al.*, 2007].

B. Topex/Poseidon (T/P)-derived water levels

The T/P radar altimeter is the first dual frequency sensor of a joint French and U.S. mission, whose goal is to substantially improve our understanding of global ocean dynamics by making accurate measurements of the ocean surface topography [*Fu and Cazenave*, 2001]. It operates in Ku and C bands, at frequencies (wavelengths) of 13.6 GHz (2.3 cm) and 5.3 GHz (5.8 cm), respectively. During its 10-day repeat cycle, T/P has provided along-track nadir measurements of Earth surface elevation (ocean and

continental surfaces) between 66° latitude north and 66° latitude south since it was launched in October 1992. Radar altimetry entails vertical range measurements between the satellite and the Earth surface. The water levels are given by the difference between the satellite orbit information and the range [*Fu and Cazenave*, 2001] or altimetric height. We use the Geophysical Data Records (standard ocean data, AVISO data base) which are commonly used for the monitoring of water levels over rivers and floodplains (e.g., *Birkett*, 1998;*Birkett et al.*, 2002; *Maheu et al.*, 2003]. The altimetry data have been corrected for the classical geophysical and environmental corrections needed over land (see for instance *Frappart et al.*, 2006b). The accuracy of T/P derived water levels in the Negro River basin is discussed in section IV A.

C. In-situ water level time series

The Brazilian Water Agency (Agencia Nacional de Aguas or ANA) is in charge of managing a network of 571 gauging stations in the Brazilian part of the Amazon basin (http://www.ana.gov.br). At each station, daily measurements of water stage are collected, and daily estimates of discharge are produced using rating curves, obtained from periodic (sometimes several times a year) simultaneous measures of stage and discharge. Among these 571 inventoried gauges, 46 are located in the Negro River sub-basin and 25 of them have records over the last 20 years. From these 25 in-situ gauge stations, only 8 are leveled and thus can be used for this study (Fig. 1). We also used daily river discharges from Jatuarana (1st in-situ station downstream the confluence of Solimões and Negro rivers) and Manacapuru (outlet of the Solimões River) to estimate by difference the monthly river discharge in Manaus.

D. GRACE-derived land water solutions

The GRACE mission, launched in March 2002, is devoted to measuring spatio-temporal changes in Earth's gravity field that results mainly from water mass redistribution among the surface fluid envelopes [*Tapley et al.,* 2004b]. Several recent studies have shown that GRACE data over the continents provide important new information on the total land water storage (surface waters, soil moisture and underground waters, and where appropriate on snow mass) [*Tapley et al.,* 2004a; *Wahr et al.,* 2004; *Chen et al.,* 2005a,b; *Ramillien et al.*, 2005; *Rodell et al.*, 2006; *Schmidt et al.,* 2006; *Yeh et al.*, 2006].

We use the land water and snow solutions derived from the inversion of 35 GRACE geoids from the third data release by GeoForschungZentrum (GFZ-RL03), as presented in *Ramillien et al.* [2005, 2006]. These solutions range from February 2003 to February 2006, with a few missing months (June 2003 and January 2004) and a spatial resolution of 400 km. Studies made with previous and less accurate releases of GRACE products estimated the error on the land water storage to be 18 mm for 750 km spatial average GRACE based land water solutions [*Wahr et al.*, 2004] and *Ramillien et al.* [2005; 2006] found an error 15 mm as the final *a posteriori* uncertainty on the land water solutions, with spatial resolution of 660 km.

E. Precipitation from GPCP

The Global Precipitation Climatology Project (GPCP), established in 1986 by the World Climate Research Program, provides data that quantify the distribution of precipitation over the whole globe [*Adler et al.*, 2003]. We use here the Satellite-Gauge Combined Precipitation Data product of GPCP Version 2 data for evaluating our

estimates of monthly surface water volume variations in the Negro River basin. The GPCP products we are using are monthly means with a spatial resolution of 2.5° of latitude and longitude and are available from January 1979 to present. Over land surfaces, the uncertainty in the rate estimates from GPCP is generally lower than over the oceans due to the *in situ* gauge input (in addition to satellite) from the GPCC (Global Precipitation Climatology Center). Over land, validation experiments have been conducted in a variety of location worldwide and suggest that while there are known problems in regions of persistent convective precipitation, non precipitating cirrus or regions of complex terrain, the estimates uncertainties range between 10%–30% [*Adler et al*., 2003].

IV. METHODS

A. Water level time series derived from T/P altimetry

Along the satellite tracks shown in Fig. 1, we have considered 86 altimetry stations at which we have computed water level time-series from T/P altimetry data. These altimetry stations are identified in Fig. 1 by the white dots. The altimetry stations selected here are those which provide good quality water level time-series (according to data editing and error bars associated with each time-series — see below) and few data gaps. Most stations are located over the floodplains. Other stations correspond to intersections of the satellite tracks with the river.

To construct a water level time series, we consider all 10 Hz altimetry data along a portion of satellite track. The intersections between satellite tracks and rivers or

floodplains were determined using the flooded areas identified by a classification of the JERS-1 dual mosaics [*Frappart et al.*, 2005]. Once selected, the data are expressed in terms of water height (water level) above the geoid (for that purpose, the GRACE geoid GGM02C, complete to degree and order 150, has been used; *Tapley et al.,* 2005). For each intersection between the river (or the floodplain) and the satellite ground track, we define a so-called 'altimetry station', represented by a rectangular window. Outliers are deleted using a 3-σ criterion over the whole time span of analysis. For each 10 day cycle, the water level at a given virtual station is obtained by computing the median of all the high-rate data (10 Hz) included in the rectangular window. This process, repeated for each cycle, allows the construction of a water level time-series at the virtual station. The dispersion in L1 norm is given by the estimator known as Median Absolute Deviation:

$$MAD(x) = \frac{1}{N-1}\sum_{i=1}^{N}\left|x_i - x_{med}\right| \qquad (1)$$

where N: number of observations, x_i : i^{th} observation, x_{med}: median of the observations.

The accuracy of T/P water level time-series over river and floodplains has been discussed in several previously published papers (i.e. *Birkett*, 1998; *de Oliveira Campos et al.,* 2001; *Birkett et al.*, 2002; *Maheu et al.,* 2003). For this study, the accuracy of the altimetry derived water levels over the Negro River was previously estimated by *Frappart et al.* [2005]. Minimum standard deviations of around 10 cm are measured on downstream rivers with large open water areas during high water when the pulse emitted by the altimeter is not scattered by vegetation, whereas maximum standard deviations of around 50 cm are observed on flooded areas covered with dense vegetation during low water.

B. Water level maps

Monthly maps of water level can be estimated over the Negro River basin. As the temporal resolution of the inundation map is one month, we create monthly averages of the water levels for each altimetry or *in situ* station. For a given month during the flood season, water levels were linearly interpolated over the flooded zones of the Negro River basin. A pixel of 25 km x 25 km is considered inundated when its percentage of inundated area is greater than 0. Maps of interpolated surface water levels with 25 km resolution have been constructed for each month between January 1993 and December 2000. As mentioned above, water levels are expressed with respect to the geoid. For the purpose of hydrological interpretation of water volumes, referring to the topography would be best as far as floodplains are concerned. However, available topographic databases are not necessarily precise enough for the present study.

The monthly maps of water level were produced by bilinear interpolation scheme to estimate the water level for each grid point.

The upstream portion of the Negro River is orientated North/South. It flows from West to East after the confluence with the Uaupes, a West/East flowing tributary, until Manaus, the outlet of the Negro River. The Branco River, the largest tributary of the Negro River, flows North/South. Two types of cross-section are observed: the satellite crosses the river and the satellite track runs along the river. As T/P crosstrack (or inter-track) is 315 km at the Equator, large floodplain areas are not measured by the altimeter. Over the western/eastern flowing parts of the river network, the T/P tracks cross the river nearly perpendicularly, allowing clear separation of the contributions of the river mainstream from those of associated floodplains (see Fig. 1). As a consequence, the

interpolation in the along-track direction follows the difference of water levels between the mainstream and the floodplain. In the cross-track direction, interpolation over several tens of kilometers will only reflect the mean slope of the river.

Over the northern/southern flowing parts of the river network, the T/P tracks run parallel to the river. In these cases, depending on the choice of the geographical coordinates of the virtual station, the time series can be influenced by the elevation variation within the adjacent floodplain [*Birkett et al.*, 2002]. These authors did not report obvious amplitude or phase differences due to the inclusion of some floodplain areas. The water levels drops between the mainstream and the inundated floodplain, as reported by *Alsdorf* [2003] using interferometric SAR observations on the Amazon floodplain (lower than 11 cm), are generally lower than the altimeter-derived water level dispersion.

C. Surface water volume

The variation of water volume corresponds to the difference of surface water levels integrated over the inundated surface. These variations $\delta V(t_i , t_{i-1})$, between two consecutive months numbered i and $i - 1$, over the floodplain S, are the sum of the products of the difference of surface water levels $\delta h_j (i , i - 1)$, with $j = 1, 2, \ldots$ inside S, by the elementary surfaces $R_e^{\,2}$ and the percentage of inundation P_j:

$$\delta V(i,i-1) = R_e^{\,2}\delta\lambda\delta\theta\sum_{j\in S} P_j \delta h_j(\theta,\lambda,i,i-1)\sin(\theta_j) \qquad (3)$$

where $\delta\lambda$ and $\delta\theta$ are the sampling grid steps along longitude λ and latitude θ (0.22°), respectively, and R_e the mean radius of the Earth (6378 km). The surface and total water volume variations are expressed in km^3/month.

The error of the method was estimated using:

$$d\delta V = \sum_{i=1}^{n} \left(dS_i \delta h_i + S_i d\delta h_i \right) \qquad (4)$$

where: $d\delta V$ is the error on the water volume variation (δV), S_i is the i^{th} elementary surface, δh_i is the i^{th} elementary water level variation between two consecutive months, dS_i is the error on the i^{th} elementary surface, and $d\delta h_i$ is the error on the i^{th} elementary water level variation between two consecutive months.

The error sources include misclassifications, T/P altimetry measurements and the linear interpolation method. The maximum error on the volume variation can be estimated as:

$$\Delta(\delta V_{\max}) \le \Delta S \max \delta h_{\max} + S_{\max} \Delta(\delta h_{\max}) \qquad (5)$$

where: $\Delta(\delta V_{max})$ is the maximum error on the water volume variation (δV), S_{max} is the maximum flooded surface, δh_{max} is the maximum water level variation between two consecutive months, ΔS_{max} is the maximum error for the flooded surface, and $\Delta(\delta h_{max})$ is the maximum error for the water level variation between two consecutive months.

V. RESULTS

A. Spatial distribution of inundated areas

The inundated area fractions for the Negro River basin were extracted from the *Prigent et al.* [2007] dataset. Note that lacking additional external information, the technique captures, but does not discriminate among, inundated wetlands, rivers, small lakes, irrigated agriculture. *Prigent et al.*, [2007] showed that this multisatellite inundation dataset exhibits very realistic distributions, with major inundated wetlands well delineated for all latitudes and environments and are considered consistent with existing independent static inventories [Prigent et al, 2001a; 2007]. Moreover, their seasonal and inter-annual variability has been evaluated over different environments and

over different large river basins with respect to rain rate and snow estimates, altimeter river height levels, and were found consistent with other related hydrological variables such as *in situ* river discharge. The only possible independent evaluation of the accuracy at regional scale was performed by comparisons with high-resolution images from Synthetic Aperture Radar and indicated only a likely underestimation of the extent of the small wetlands (< 80 km^2, ie ~10% of a ~800 km^2 pixel of our equal-area grid (see figure 6 and 7 of *Prigent et al*. [2007]).

Fig. 2 shows the average fractional inundation in the Negro River basin for 1994. The areas with a very high percentage of inundation (greater than 50%) are located on the lower part of the Negro River and the confluence between Negro and Branco rivers. The pixels corresponding to open waters, temporarily flooded pastures and low vegetation submerged by water during the flood in the Caracarai sub-basin (upper part of the Branco River) also exhibit a large percentage of inundation (between 20 and 70%). Inundation associated with Negro River basin is well captured, even in complex regions characterized by extensive flooding below dense vegetation canopies, with potentially high fractional inundation extent, low variability in the annual maximum, and quasi-permanent flooding (Fig. 2).

The seasonal and interannual variations of total inundated area in the Negro River basin are presented on Fig. 3. The maximum is observed from May to July whereas the minimum is observed from November to February. Fig. 3 shows important interannual variability with maximum inundated area varying from 57,000 km^2 (June 1996) to 42,000 km^2 (June 1997) and minimum inundated area varying from 28,000 km^2 (January 1997) to 15,700 km^2 (December 1997), while 1998 is characterized by an important peak of

inundated area (53,500 km^2) which occurs after a year of very small inundation area. The small inundation in 1997 and large inundation in 1998 corresponds to the 1997/1998 El Niño Southern Oscillation (ENSO) event and its opposite (1998/1999 La Niña) which are associated with decreases and increases of water levels and discharge in the Negro River basin [*Guyot et al.*, 1998] and water storage in the whole Amazon basin [*Stuck et al.*, 2006].

Long-term and higher spatial resolution surveys of wetland extent over large regions are very scarce. SAR imagery can provide estimates with much better spatial resolution than the multisatellite inundation product but suffers from a lack of temporal coverage. One study of flooding in the Amazon basin for both low-water (September–October 1995) and high-water (May–June 1996) conditions is that of *Frappart et al.* [2005] based on 100-m resolution L-band SAR observations from the Japanese Earth Resources Satellite-1 (JERS-1). Table 1 compares our estimates with the *Frappart et al.* [2005] results during low (October 1995) and high water (June 1996) for the Negro River. The total SAR-derived flooded area is 36,000 km^2 (159,000 km^2) for this 700,000 km^2 region as compared to our results of 26,000 km^2 (57,000 km^2) for low (high) water stage. The difference in total flooded area is larger during high water stage. With its much better spatial resolution, the SAR can more accurately estimate small areas that are flooded in generally dry conditions or small dry areas in generally flooded conditions, whereas our lower resolution observations may miss some fractional coverage. Nevertheless, due to the low sensibility of L-Band to smooth surfaces, is responsible for a loss of accuracy for the discrimination between open water surfaces, bare soils and low vegetated areas [*Martinez and Le Toan*, 2007]. Besides, sensitivity analysis showed that the classification

accuracy is highly dependant on the number of images used (Martinez and Le Toan, 2007). The classification results used here for delineating the floodplains in the Negro River basin were obtained with only two acquisitions of SAR images (JERS-1 double mosaic), i.e., the worst configuration in terms of accuracy.

The SAR-derived product presents a greater sensitivity to small amounts of water under dense canopy cover than the multisatellite product. The inundation of the upper Negro (Cucui and Sao Felipe sub-basins) and Uaupes (Serrinha sub-basin) are underestimated by the multisatellite dataset. Without the flooded area of these three sub-basins, the SAR-derived flooded areas are now 25,000 km^2 and 95,000 km^2 for low and high water stage respectively. The two estimates are almost identical for low water stage but the SAR-derived remains greater at high water stage.

Additionally, as shown in *Prigent et al*. [2007], during the low water stage, more pixels with low fractional inundation are detected by the SAR relative to our product, but also there is a tendency for our analysis to overestimate the higher fractional inundations as well. However, both of these biases are smaller during high water stage. This result may be explained by more frequent areas with small fractional inundation during low water stage, as expected, but also by the more frequent occurrence of small dry patches in areas with large fractional inundation. However, a very strict detection threshold produces a systematic overestimate, whereas a less strict threshold allows for both overestimates and underestimates, producing a small average error. Likewise, our lower-resolution product can yield a less biased estimate using a finite detection threshold as we did. We note that the SAR product still has some artifacts that have not been removed (radar speckle, lagged gain changes) and that the boundary between flooded and dry

signals is still somewhat ambiguous [*Hess et al.*, 2003], as in our analysis, so there is uncertainty in the detection threshold for SAR as well.

B. Water level time series

The 86 T/P altimetry stations where water level time series can be constructed are unevenly distributed across the basin (Fig. 1). Thirty-two are located on rivers and 54 on wetlands. An important goal of this dataset is to give valuable information on water levels for unmonitored regions of the Negro River basin such as the Uaupes River flowing from the Colombian part of the watershed, on the western side of the Negro basin (four stations on the river and one on the floodplain), the upper Negro, near the Venezuelan border and the divide with Orinoco basin (15 mainly on a large unmonitored inundated area), or the right bank of Negro River (9 stations). Examples of water level time series derived from radar altimetry are presented on Fig. 4.

This relatively large number of stations (94 encompassing 86 altimetric and 8 in-situ), distributed over river channels and wetlands, is necessary to estimate accurately water volume variations. *Frappart et al*. [2005] reported that the precision is better on the river channels than on the inundated areas and floodplains. Minimum standard deviations of around 10 cm are measured on downstream rivers with large open water areas when the pulse emitted by the altimeter is not scattered by vegetation, whereas maximum standard deviations of around 60 cm is observed on flooded areas covered with dense vegetation.

C. Water volume variations

The monthly flood maps indicate that the flood period in the Negro River generally ranges from May to August, whereas low water period ranges from September to February. As an example for the 95-96 hydrological cycle, Fig. 5 shows maps of interpolated water levels for October 1995 and June 1996, which corresponds to the minimum and maximum respectively.

Figure 6 presents the differences between two consecutive months of the mean surface water volume (i.e. the monthly change in floodplain water storage) averaged over the study area for 1993-2000. Positive variations are obtained between November and June. They are more important for the years 1996 and 1998. We also calculated the water storage changes during the 1995-1996 hydrological cycle of the Negro river. It corresponds to a volume variation of 167 km^3 for the whole floodplain.

Using (5), we have estimated the maximum error on the volume change in the lower Negro River basin with the following values:

S_{max} = 60,000 km^2 in year 2000 (cf. Fig. 3),

δh_{max} = 5 m, maximum water level change between two consecutive months during the study period,

ΔS_{max} = 10% (cf. Prigent et al., 2007) of 60,000 km^2,

$\Delta(\delta h_{max})$ = 0.5 m, maximum dispersion of the altimeter measurements.

For the whole study zone, we obtained a maximum error of 39 km^3 over the period October 1995 – June 1996 for a total positive variation of 167 km^3, that is to say an error of 23%.

Comparisons have been made with the results obtained combining T/P altimetry and JERS-1 imagery [*Frappart et al.*, 2005]. The results of this comparison are presented in Table 2. The total SAR-derived flooded volume difference between low and high water stages is 320 km^3, that is to say almost two times larger than our current results. If the

sub-basins of Cucui, Sao Felipe and Serrinha are not included in the estimate for the reasons previously mentioned, the maximum storage is 220 km^3. For the same study area, our result is 30% lower than the maximum storage variations estimated by *Frappart et al.* [2005]. The difference of maximum of surface water storage variations between the two methods mainly come from the difference between the flooded area estimates.

We then compared the mean annual cycle of monthly surface storage variations for 1993-2000 period with the mean annual cycle of monthly changes in total water storage from GRACE for 2003-2005 (Figure 7). We notice that the average monthly GRACE-derived total water volume changes present almost in-phase fluctuations with the average monthly changes in surface water volume computed in the present study. The maxima and minima of the time-series are observed the same month, May and October respectively. The maximum surface water volume change represents between a third and a half of the total and the minimum roughly a half.

A comparison between water volume stored in the floodplains of the Negro River basin and the water volume that flows to Manaus (outlet of the basin) was performed. The time series of monthly changes in surface water volume and monthly integrated discharge are presented in Figure 8. The two time series present the same range of variations (between -80 km^3/month and 50 km^3/month). Nevertheless, no obvious relationship can be found between these two parameters. *Frappart et al.* [2005] already observed this lack of clear relationship between potential storage capacity within the floodplain and integrated discharge during the flood season.

Figure 9 compares the time series of the monthly changes in surface water volume and monthly variations of precipitation in the Negro River Basin for the period 1993 -

2000. Both exhibit a similar behavior with a correlation of 0.61 for a time lag of one month (precipitation precedes surface storage variations), although precipitation variations are lower than surface water volume between January and March for years 1994, 1995 and 1998.

The surface water changes averaged over a river basin can be removed from the total water changes detected by the GRACE gravimetry mission to estimate monthly changes in water stored in the rest of the Negro River basin (i.e. soil moisture and groundwater). Due to the lack of a common period between the estimated surface water volume variations and GRACE observations, we compared the annual cycle of monthly-average surface storage variations for 1993-2000 with the annual cycle of changes in total storage from GRACE for 2003-2005. Figure 10 shows difference between these two, or the monthly changes in basin water storage outside of the river channel/floodplain system. The climatology hence defined showed that the total water storage of the Negro River basin is almost equally partitioned between surface water and the combination of soil moisture and groundwater.

CONCLUSION

In this study, we estimated surface water storage variations in the Negro River for the 1993-2000 period. The combined use of altimetric water level observations (from T/P) and inundation patterns derived from multi-satellite information to determine water volume variations provides valuable information on the inundation dynamics of river floodplains. Seasonal and interannual variabilities are consistent with precipitation and rivers discharge and especially during ENSO years.

Knowledge of surface water volumes has several potential applications, as flood monitoring and forecasting, sediment and nutrient transport assessment or floodplain geomorphology.

We also demonstrate the complementarity between several types of remote sensing data: multisatellite inundation dataset, water levels derived from radar altimetry and GRACE measurements of the total water storage. For the first time, a decomposition into several components of the total water storage from GRACE is shown to be possible.

These results will have implications for better monitoring the water cycle, and in particular improvements can be expected when additional data from current and future satellite missions are used. The combination of data from the present radar altimeters (T/P, ERS-1&2, Jason-1, ENVISAT RA-2) will allow better sampling of water level variations over rivers and floodplains in both time and space. The use of the future soil moisture products derived from the SMOS (Kerr et al., 2001) and future soil moisture missions will allow for further decomposition of the change in total water storage into its surface water, soil moisture and remaining storage reservoirs (e.g. groundwater).

Acknowledgments

The authors would like to acknowledge the CTOH (Centre de Topographie des Océans et de l'Hydrosphère) at LEGOS for the provision of the Topex/Poseidon GDR dataset and the HYBAM project for the in-situ gauge measurements. The first and third authors were supported by NASA Gravimetry Recovery and Climate Experiment (GRACE) Hydrology grants.

REFERENCES

Adler, R. F., G. J. Huffman, A. Chang, R. Ferraro, P. Xie, J. Janowiak, B. Rudolf, U. Schneider, S. Curtis, D. Bolvin, A. Gruber, J. Susskind, and P. Arkin (2003), The Version 2 Global Precipitation Climatology Project (GPCP) Monthly Precipitation Analysis (1979-Present), *J. Hydrometeor*., *4*,1147-1167.

Alsdorf, D. E., J. M. Melack, T. Dunne, L. K. Mertes, L. L. Hess , and L. C. Smith (2000), Interferometric radar measurements of water level changes on the Amazon floodplain, *Nature, 404*, 174-177.

Alsdorf, D. E., L. C. Smith and J. M. Melack (2001), Amazon floodplain water level changes measured with interferometric SIR-C radar, *IEEE Trans. Geosci. Remote Sensing, 39 (2)*, 423-431.

Alsdorf, D. E. (2003), Water storage of the central Amazon floodplain measured with GIS and remote sensing imagery, *Annals of the Association of American Geographers, 93 (1)*, 55-66.

Alsdorf, D. E., and D. P. Lettenmaier (2003), Tracking fresh water from space, *Science, 301,* 1492-1494.

Alsdorf,, D. E., P. Bates, J. Melack, M. Wilson, and T. Dunne (2007), Spatial and temporal complexity of the Amazon flood measured from space, *Geophys. Res. Lett*., 34, L08402, doi:10.1029/2007GL029447.

Birkett, C. M. (1998), Contribution of the TOPEX NASA radar altimeter to the global monitoring of large rivers and wetlands, *Water Resour. Res., 34 (5)*, 1223-1239.

Birkett, C. M., L. A. K. Mertes, T. Dunne, M. H. Costa, and M. J. Jasinski (2002), Surface water dynamics in the Amazon Basin : Application of satellite radar altimetry, *J. Geophys. Res., 107 (D20)*, 8059-8080.

Bousquet, P., P. Ciais, J. B. Miller, E. J. Dlugokencky, D. A. Hauglustaine, C. Prigent, G.R. Van der Werf, P. Peylin, E.G. Brunke, C. Carouge, R. L. Langenfelds, J. Lathière, F. Papa, M. Ramonet, M. Schmidt, L. P. Steele, S. C. Tyler, and J. White (2006), Contribution of anthropogenic and natural sources to atmospheric methane variability. *Nature*, *443*, 439-443, doi:10.1038/nature05132.

Cao,, Z., M. Wang, B. Proctor, G. Strong, R. Stewart, H. Ritchie, and J. E. Burford (2002), On the physical processes associated with the water budget and discharge

over the Mackenzie basin during the 1994/95 water year, *Atmosphere-Ocean, 40(2)*, 125-143.

Chen, J. L., C. R. Wilson, J. S. Famiglietti, and M. Rodell (2005a), Spatial sensitivity of the Gravity Recovery and Climate Experiment (GRACE) timevariable gravity observations, *J. Geophys. Res., Solid Earth,* 110**,** B08408.

Chen, J., M. Rodell, C. R. Wilson, and J. S. Famiglietti (2005b), Low degree spherical harmonic influences on Gravity Recovery and Climate Experiment (GRACE) water storage estimates, *Geophys. Res. Lett., 32*, L14405, doi:10.1029/2005GL022964.

Cosandey, C., and M. Robinson (2000), Hydrologie continentale, *coll. U, Armand Colin, Paris*, 360 p..

Coe, M. T., M. H. Costa, A. Botta, and C. Birkett (2002), Long-term simulations of discharge and floods in the Amazon Basin, *J. Geophys. Res.*, 107(D20), 8044, doi:10.1029/2001JD000740.

Decharme, B., H. Douville, C. Prigent, F. Papa, and F. Aires (2007), A new river flooding scheme for global climate applications Off-line validation over South America, *J. Geophys. Res*., submitted.

Famiglietti, J. S. (2004), Remote Sensing of Terrestrial Water Storage, Soil Moisture and Surface Waters, in *The State of the Planet: Frontiers and Challenge*s *in Geophysics*, Geophysical Monograph Series, Volume 150, R. S. J. Sparks and C. J. Hawkesworth, eds., pp. 197-207.

Frappart, F., J. M. Martinez, F. Seyler, J. G. León, and A. Cazenave (2005), Floodplain water storage in the Negro River basin estimated from microwave remote sensing of inundation area and water levels, *Remote Sens. Environ., 99*, 387-399.

Frappart, F., K. Do Minh, J. L'Hermitte, A. Cazenave, G. Ramillien, T. Le Toan, N. Mognard-Campbell (2006 a), Water volume change in the lower Mekong basin from satellite altimetry and imagery data, *Geophys. J. Int, 167 (2)*, 570-584, doi:10.1111/j.1365-246X.2006.03184.x.

Frappart, F., S. Calmant, M. Cauhopé, F. Seyler, and A. Cazenave (2006 b), Preliminary results of ENVISAT RA-2 derived water levels validation over the Amazon basin, *Remote Sens. Environ.,100*, 252-264.

Fu L.L., and A. Cazenave (2001), Satellite altimetry and Earth science, a handbook of techniques and applications, *Academic Press*, London, U.K.

Guyot, J. L., J. Callède, M. Molinier, V. Guimarães, and E. De Oliveira (1998), La variabilité hydrologique actuelle dans le bassin de l'Amazone, *Bulletin de l'Institut Français d'Etudes Andines*, 27 (3), 779-788.

Hess, L. L., J. M. Melack, E. M. L. M. Novob, C. C. F. Barbosac, and M. Gastil (2003), Dual-season mapping of wetland inundation and vegetation for the central Amazon basin, *Remote Sens. Environ., 87*, 404-428.

James, M. E., and S. N. V. Kalluri, (1994), The Pathfinder AVHRR land data set: An improved coarse resolution data set for terrestrial monitoring, *Int. J. Remote Sens., 15*, 3347-3364.

Junk W., P. B. Bayley, and R. E. Sparks (1989), The flood pulse concept in river floodplain systems, *in D.P. Dodge (Ed.) Proceedings of the International Large River Symposium. Can. Spec. Pub. Fish. Aquat. Sci. 106*, 110-127.

Kalnay, E., M. Kanamitsu, R. Kistler *et al*., (1996), The NCEP/NCAR 40-year reanalysis project, *Bull. Am. Meteorol. Soc.*, *77*, 437-470.

Kerr, Y. H., P. Waldteufel, J.-P. Wigneron, J.-M. Martinuzzi, J. Font, and M. Berger (2001),SoilMoisture Retrieval from Space: The Soil Moisture and Ocean Salinity (SMOS) Mission, *IEEE Trans. Geosci. Rem. Sens., 39*, 1729-1735.

Lettenmaier, D. P., and J. S. Famiglietti (2007), Water from on high, *Nature, 444*, 562-563.

Liebmann, B., and J. A. Marengo (2001), Interannual variability of the rainy season and rainfall in the Brazilian Amazon basin, *J. Clim., 14*, 4308-4318.

Lyon, B. (2004), The strength of El Nino and the spatial extent of tropical drought, *Geophys. Res. Lett., , 31*, L21204, doi:10.1029/2004GL020901.

Maheu, C., A. Cazenave A., and C. R. Mechoso (2003), Water level fluctuations in the Plata basin (South America) from Topex/Poseidon satellite altimetry, *Geophys. Res. Let., 30 (3),* 1143-1146.

Maltby E. (1991). Wetland management goals: wise use and conservation, *Landscape Urban Plan., 20*, 9-18.

Marengo, J. A., B. Liebmann, V. E. Kousky, Filizola, and I. C. Wainer. (2001), Onset and end of the rainy season in the Brazilian Amazon basin, *J. Clim., 14*, 833-852.

Marsily, G. de (2005), Eaux continentales, *C. R. Geoscience, 337*, 1-2.

Martinez J. M. and T. Le Toan (2007), Mapping of Flood Dynamics and Spatial Distribution of Vegetation in the Amazon Floodplain Using Multitemporal Sar Data, *Remote Sens. Env.,108 (3)*, 209-223.

Matthews, E. (2000*), Wetlands in Atmospheric methane: its role in the global environment*, edited by M. A. K. Khalil, pp. 202-233, Springer-Verlag, New York.

Meade, R.H., J. M. Rayol, S. C. Conceicão da Natividade (1991), Backwater effects in the Amazon River basin of Brazil, *Environ. Geol. Water Sci., 18 (2)*, 105-114.

Mercier, F., A. Cazenave, and C. Maheu (2002), Interrannual lake level fluctuations (1993-1999) in Africa from Topex/Poseidon : connections with ocean-atmosphere interactions over the Indian Ocean*, Global and Planetary Changes, 32,* 141-163.

Molinier, M., J. L. Guyot, E. de Oliveira, V. Guimarães, and A. Chaves (1995), Hydrologie du basin de l'Amazone, in Olivry J.C et J Boulègue (eds) : *Grands bassins fluviaux péri-atlantiques : Congo, Niger, Amazone*. Actes du Colloque PEGI/INSU/CNRS.ORSTOM, Paris, France, 22-24 novembre 1993, pp. 335-344.

OECD (1996), *Guidelines for aid agencies for improved conservation and sustainable use of tropical and sub-tropical wetlands*, Organisation for Economic Cooperation and Development, Development Assistance Committee: Guidelines on Aid and Environment, 9, 69 pp.

Oliveira Campos, I . de, F. Mercier, C. Maheu, G. Cochonneau, P. Kosuth, D. Blitzkow, and A. Cazenave (2001), Temporal variations of river basin waters from Topex/Poseidon satellite altimetry ; application to the Amazon basin, *C.R. Acad. Sci. Paris, Sciences de la Terre et des planètes, 333,* 1-11.

Papa, F., C. Prigent, F. Durand, and W. B. Rossow (2006b), Wetland dynamics using a suite of satellite observations: A case study of application and evaluation for the Indian Subcontinent. *Geophys. Res. Lett., 33*, L08401, doi:10.1029/2006GL025767.

Papa, F., C. Prigent, and W. B. Rossow (2007a), Ob' River flood inundations from satellite observations: A relationship with winter snow parameters and river runoff, *J. Geophys. Res., 112*, D18103, doi:10.1029/2007JD008451

Papa, F., C. Prigent, and W. B. Rossow (2007b), Response of large Siberian rivers' discharge to flood variations, Rev. Geophys., submitted.

.

Perrier A., and A. Tuzet (2005), Le cycle de l'eau et les activités au sein de l'espace rural, *C. R.Geoscience*, 337, 39-56

Prigent, C., E. Matthews, F. Aires, and W. B. Rossow (2001a), Remote sensing of global wetland dynamics with multiple satellite data sets, *Geophys. Res. Lett.*, *28* , 4631-4634.

Prigent, C., F. Aires, W. B. Rossow, and E. Matthews (2001b), Joint characterization of vegetation by satellite observations from visible to microwave wavelength: A sensitivity analysis, *J. Geophys. Res*, *106*, 20665-20685.

Prigent, C., F. Aires, and W. B. Rossow, Land surface microwave emissivities over the globe for a decade, *Bul. Amer. Meteorol. Soc.,* doi:10.1175/BAMS-87-11-1573, 1573-1584, 2006.

Prigent, C., F. Papa, F. Aires, W.B. Rossow, and E. Matthews (2007), Global inundation dynamics inferred from multiple satellite observations, 1993-2000, *J. Geophys. Res.*, *112*, D12107, doi:10.1029/2006JD007847.

Ramillien, G., F. Frappart, A. Cazenave, and A. Güntner (2005), Time variations of the land water storage from an inversion of 2 years of GRACE geoids, *Earth Planet. Sci. Lett.*, *235*, 283-301.

Ramillien, G., F. Frappart, A. Cazenave, A. Güntner, and K. Laval (2006). Time variations of the regional evapotranspiration rate from Gravity Recovery and Climate Experiment (GRACE) satellite gravimetry, *Water Resour. Res., 42(10)*, W10403, 10.1029/2005WR004331.

Rango, A. (1997), Response of areal snow cover to climate change in a snowmelt-runoff model, *Annals of Glaciology, 25*, 232-236.

J. E. Richey, L. A. K. Mertes, T. Dunne, R. L. Victoria, B. R. Forsberg, A. C. M. S. Tancredi and E. Oliveira. (1989). Sources and routing of the Amazon River flood wave, *Global Biogeochem. Cycles, 3*, 191-204.

Richey, J. E., J. M. Melack, K. Aufdenkampe, V. M. Ballester, and L. Hess (2002), Outgassing from Amazonian rivers and wetlands as a large tropical source of atmospheric CO2, *Nature, 416*, 617-620.

Rodell, M., J. Chen, H. Kato, J. Famiglietti, J. Nigro, and C. Wilson (2006), Estimating ground water storage changes in the Mississippi river basin using GRACE, *Hydrogeology J.*, doi 10.1007/s10040-006-0103-7.

Rossow, W. B., and R. A. Schiffer, (1999) Advances in understanding clouds from ISCCP, *Bull. Am. Meteorol. Soc., 80*, 2261-2287.

Schmidt, R., F. Flechtner, C. Reigber, P. Schwintzer, A. Güntner, P. Döll, G. Ramillien, A. Cazenave, S. Petrovic, H. Jochman, and J. Wunsch (2006), GRACE observations of changes in continental water storage, *Glob. And Plan. Change, 50***,** 112–126.

Seo, K.-W., C. R. Wilson, J. S. Famiglietti, J. L. Chen, and M. Rodell (2006), Terrestrial water mass load changes from Gravity Recovery and Climate Experiment (GRACE), *Water Resour. Res., 42*, W05417, doi:10.1029/2005WR004255.

Sippel, S. J., S. K. Hamilton, J. M. Melack, and E. M. M. Novo (1998), Passive microwave observations of inundation area and the area/stage relation in the Amazon River floodplain, *Int. J. Remote Sens., 19*, 3055–3074.

Smith, L.C. (1997), Satellite remote sensing of river inundation area, stage and discharge: a review, *Hydrol. Process., 11*, 1427-1439.

Sternberg, H. (1975), The Amazon River of Brazil, *Geographische Zeitschrif*, 1-74.

Stuck, J., A. Güntner, and B. Merz (2006), ENSO impact on simulated South American hydro-climatology, *Advances in Geosciences, 6,* 227-236.

Syed, T. H., J. S. Famiglietti, M. Rodell, J. Chen, and C. R. Wilson (2007), Terrestrial Hydroclimatology from GRACE and GLDAS, in revision, *Wat. Resour. Res.*.

Tapley, B.D., S. Bettadpur, J. C. Ries, P. F. Thompson, and M. Watkins (2004a), GRACE measurements of mass variability in the Earth system, *Science, 305*, 503-505.

Tapley, B. D., S. Bettadpur, M. Watkins, and C. Reigber (2004b), The Gravity Recovery and Climate Experiment : Mission overview and Early results, *Geophys. Res. Lett., 31*, L09607, doi:10.1029/2004GL019920.

Tapley, B., Ries J., Bettadpur S., Chambers D., Cheng M., Condi F., Gunter B., Kang Z., Nagel P., Pastor R., Pekker T., Poole S., Wang F. (2005), GGM02 - an improved Earth gravity field model from GRACE, *J. Geod.,* 79, doi:10.1007/s00190-005-0480-z, 467–478.

Wahr, J., S. Swenson, V. Zlotnicki, and I. Velicogna (2004), Time-variable gravity from GRACE : first results, *Geophys. Res. Lett.*, 31, L11501, doi:10.1029/2004GL019779.

Winsemius, H. C, H. H. G. Savenije, A. M. J. Gerrits, E. A. Zapreeva, and R. Klees (2006), Comparison of two model approaches in the Zambezi River basin with regard to model reliability and identifiability, *Hydrol. Earth Syst. Sci., 10*, 339–352.

Yeh, P. J.-F., S. C. Swenson, J. S. Famiglietti, and M. Rodell (2006), Remote sensing of groundwater storage changes in Illinois using the Gravity Recovery and Climate Experiment (GRACE), *Water Resour. Res., 42*, W12203, doi:10.1029/2006WR005374

Table Captions

Table 1: Estimates of the flooded areas in the Negro River basin for October 1995 and June 1996 from the multisatellite product, a classification of JERS-1 images, the same classification without the upper Negro (Cucui and Sao Felipe sub-basins) and Uaupes (Serrinha sub-basin).

Table 2: Estimates of the water volume variations in the Negro River basin between October 1995 and June 1996 from the multisatellite product, a classification of JERS-1 images, the same classification without the upper Negro (Cucui and Sao Felipe sub-basins) and Uaupes (Serrinha sub-basin).

Figure Captions

Figure 1: Overview map of the Negro River basin in South America. The Negro River sub-basin from JERS-1 radar mosaic. The thick white line represents the boundary of the Negro River. Each thin white line accounts for a Topex/Poseidon track. Black dots in a white circle represent in-situ gauge stations, black dots in a white square, altimetric stations over the Negro River sub-basin.

Figure 2: Extent of inundation as estimated from the multi-satellite dataset for 1994 (% of inundated area per pixel).

Figure 3: Monthly inundated surfaces (km^2) in the Negro River basin between January 1993 to December 2000.

Figure 4: Examples of time series of water level for river (upper panel) and floodplain (lower pannel). The thin black line on the lower pannel represents the water level variations at Manaus in-situ gauge station.

Figure 5: Water level maps (with reference to GGM02C geoid) for October 1995 (a) and June 1996 (b).

Figure 6: Variation of surface water volume change from T/P radar altimetry and multi-satellite derived inundation dataset.

Figure 7: Monthly variation of surface water volume change from T/P radar altimetry and multi-satellite derived inundation dataset averaged over 1993-2000 period (black line) and monthly variation of total land water volume change from GRACE averaged over 2003-2005 period (black dotted line).

Figure 8: Monthly variation of surface water volume change from T/P radar altimetry and multi-satellite derived inundation dataset (black line) and monthly variation of volume change from integrated river discharge in Manaus (black dotted line).

Figure 9: Monthly variation of surface water volume change from T/P radar altimetry and multi-satellite derived inundation dataset (black line) and monthly precipitation rate over the Negro River basin from GPCP (black dotted line).

Figure 10: Monthly variation of surface water volume change from T/P radar altimetry and multi-satellite derived inundation dataset averaged over 1993-2000 period (blue dotted line) and monthly variation of total land water volume change from GRACE averaged over 2003-2005 period (red dotted line). The difference, which represents the sum of soil moisture and groundwater is represented by a dotted green line.

Table 1:

Flooded area (km^2)	Multi-satellite	JERS-1	JERS-1 Negro downstream
Low water (Oct 95)	26,000	36,000	25,000
High water (Jun 96)	57,000	159,000	95,000

Table 2:

	Multi-satellite	JERS-1	JERS-1 Negro downstream
dV (km^3)	167	320	220

Figure 1:

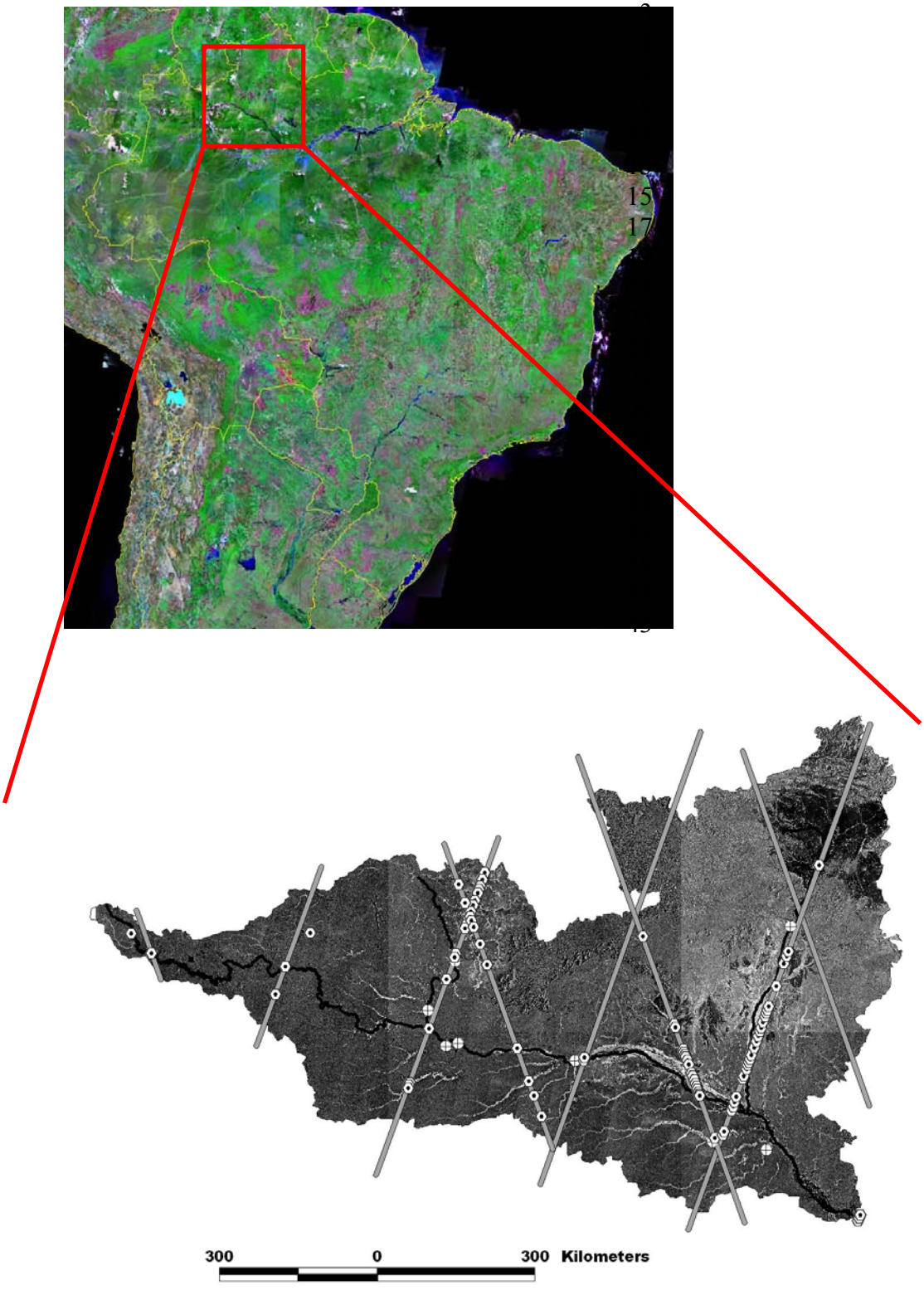

Figure 2:

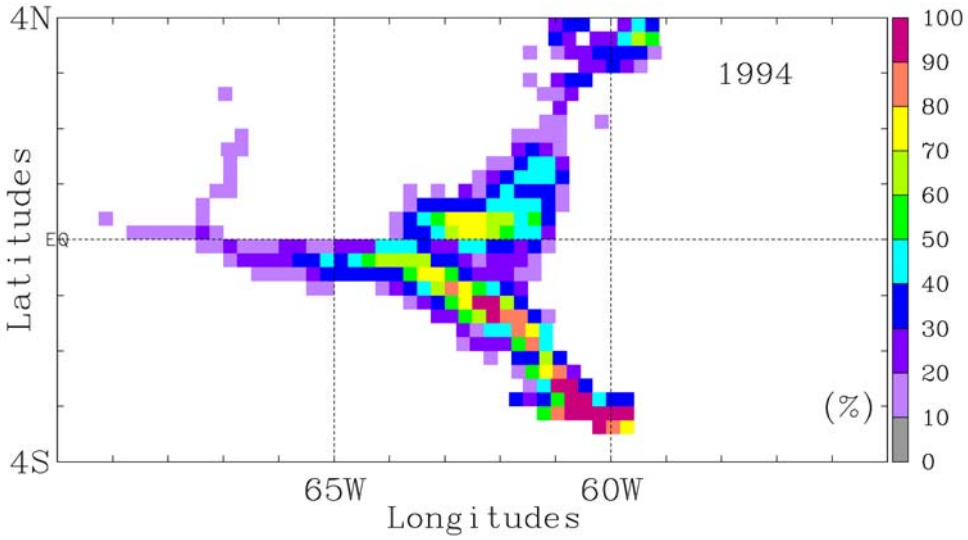
4N
EQ
4S
Latitudes
65W
60W
Longitudes
1994
(%)
100
90
80
70
60
50
40
30
20
10
0

Figure 3:

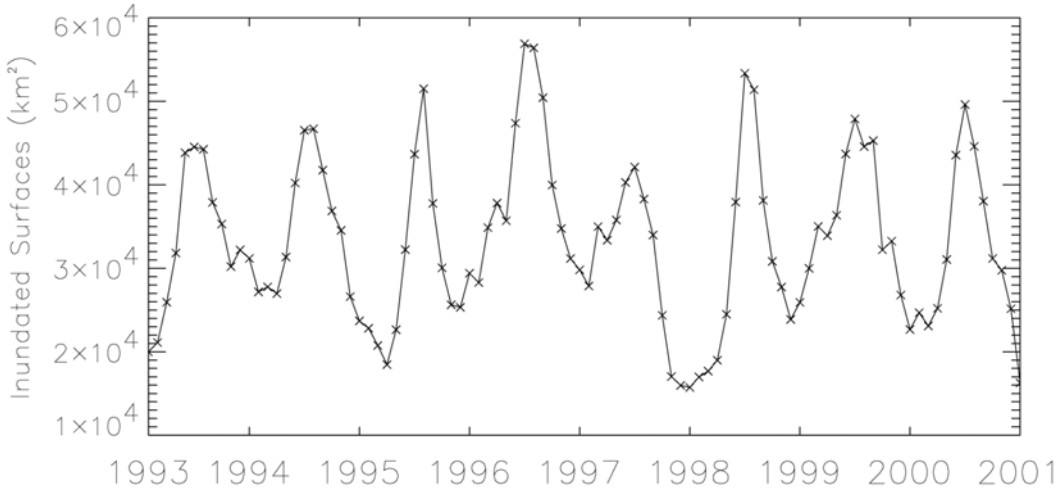
Inundated Surfaces (km²)
6×10⁴
5×10⁴
4×10⁴
3×10⁴
2×10⁴
1×10⁴
1993
1994
1995
1996
1997
1998
1999
2000
2001

1 Figure 4:
2

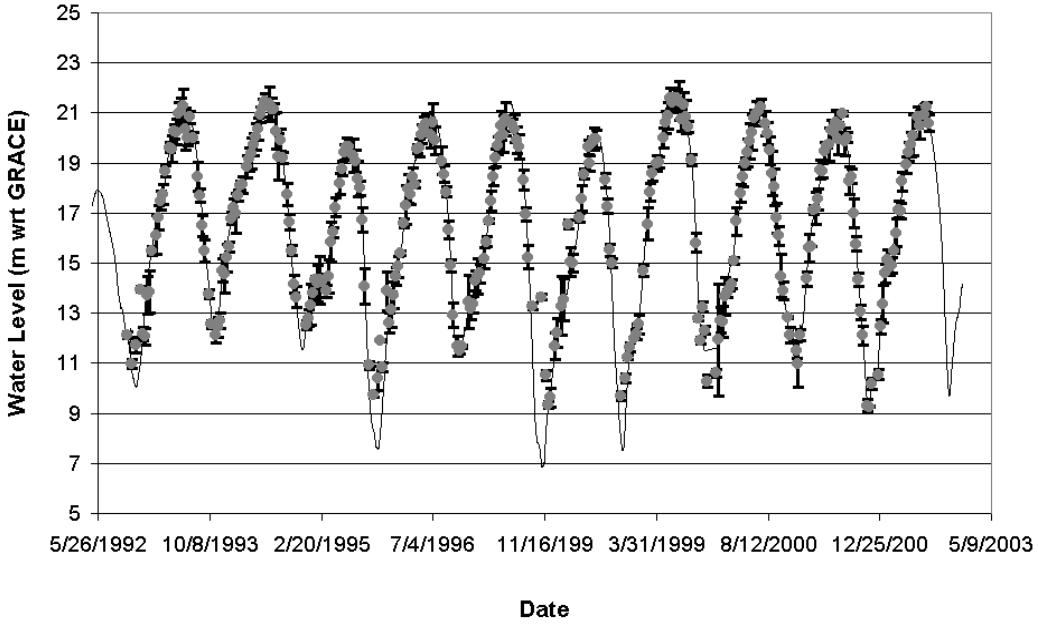
Water Level (m wrt GRACE)
25
23
21
19
17
15
13
11
9
7
5
5/26/1992
10/8/1993
2/20/1995
7/4/1996
11/16/199
3/31/1999
8/12/2000
12/25/200
5/9/2003
Date

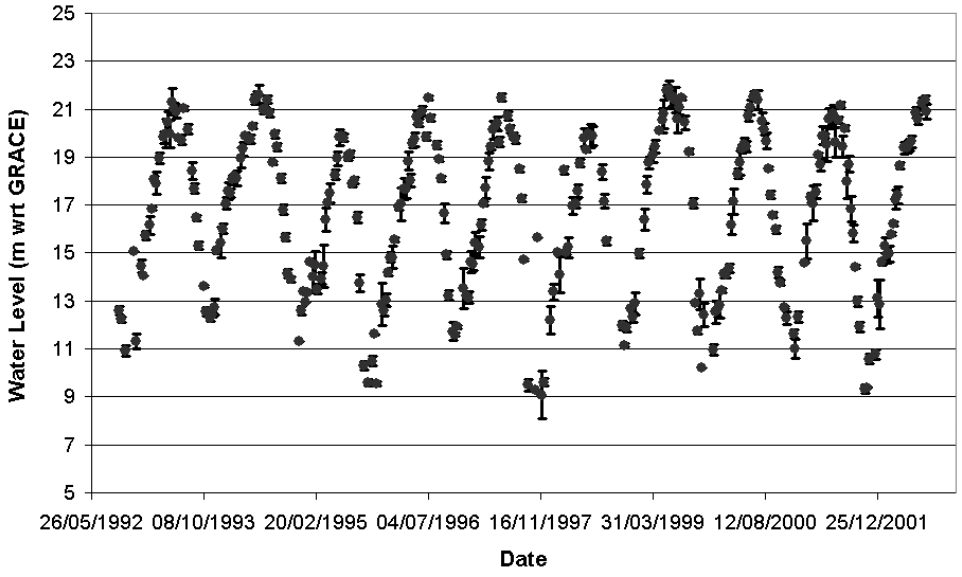
Water Level (m wrt GRACE)
25
23
21
19
17
15
13
11
9
7
5
26/05/1992
08/10/1993
20/02/1995
04/07/1996
16/11/1997
31/03/1999
12/08/2000
25/12/2001
Date

1 Figure 5:
2
3

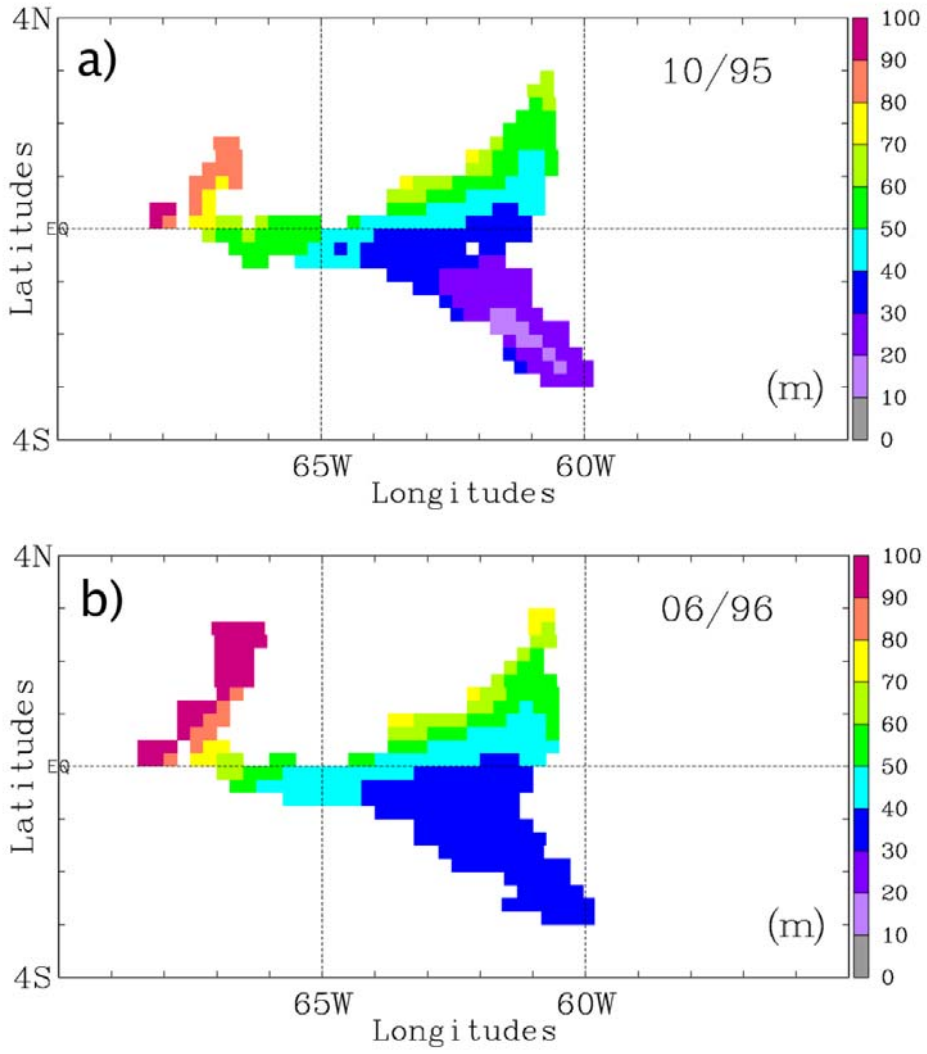
a)
10/95
(m)
4N
Latitudes
EQ
4S
65W
60W
Longitudes
100
90
80
70
60
50
40
30
20
10
0
b)
06/96
(m)
4N
Latitudes
EQ
4S
65W
60W
Longitudes
100
90
80
70
60
50
40
30
20
10
0

Figure 6:

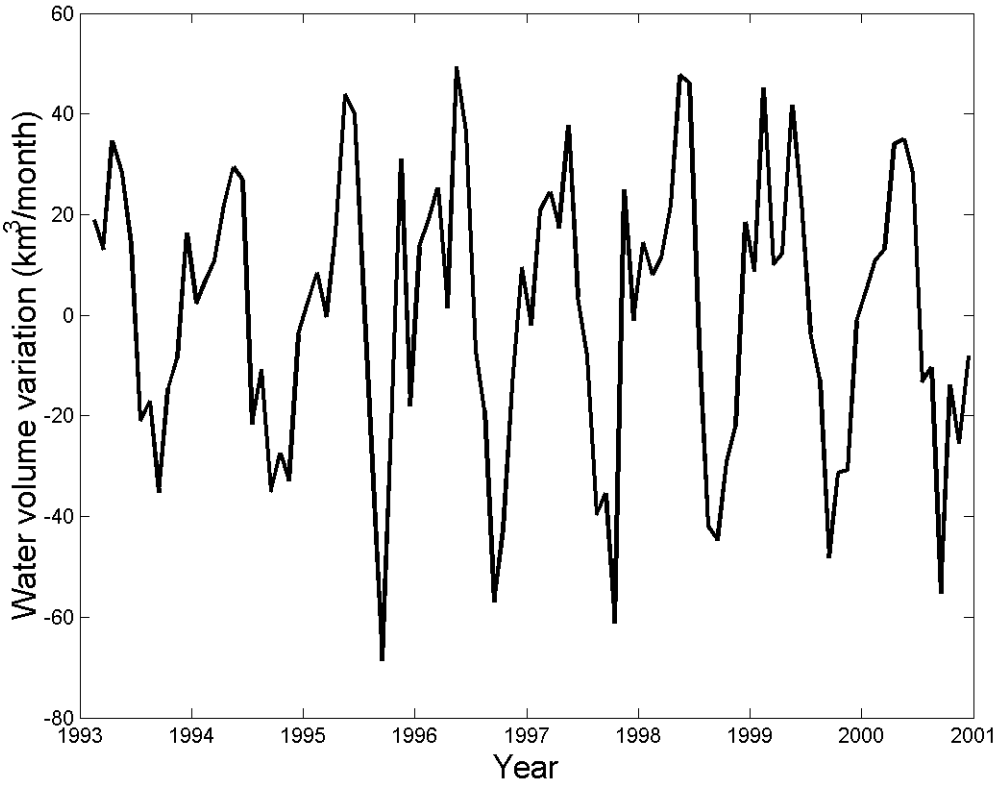
Water volume variation (km3/month)
Year
60
40
20
0
-20
-40
-60
-80
1993
1994
1995
1996
1997
1998
1999
2000
2001

Figure 7:

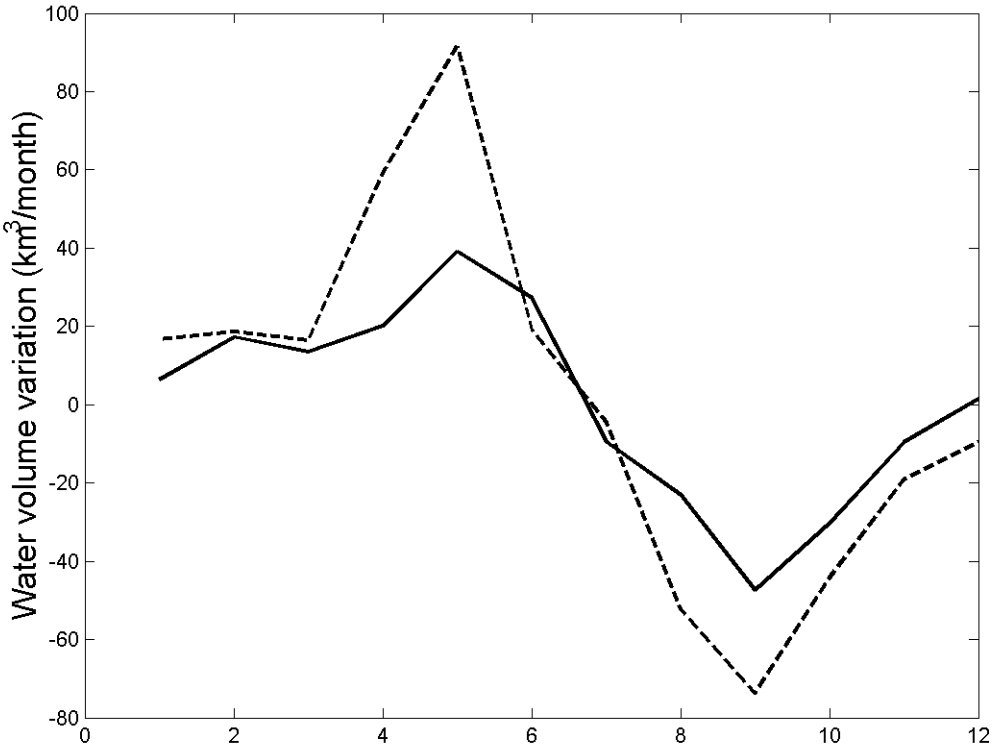
Water volume variation (km3/month)
100
80
60
40
20
0
-20
-40
-60
-80
0
2
4
6
8
10
12

Figure 8:

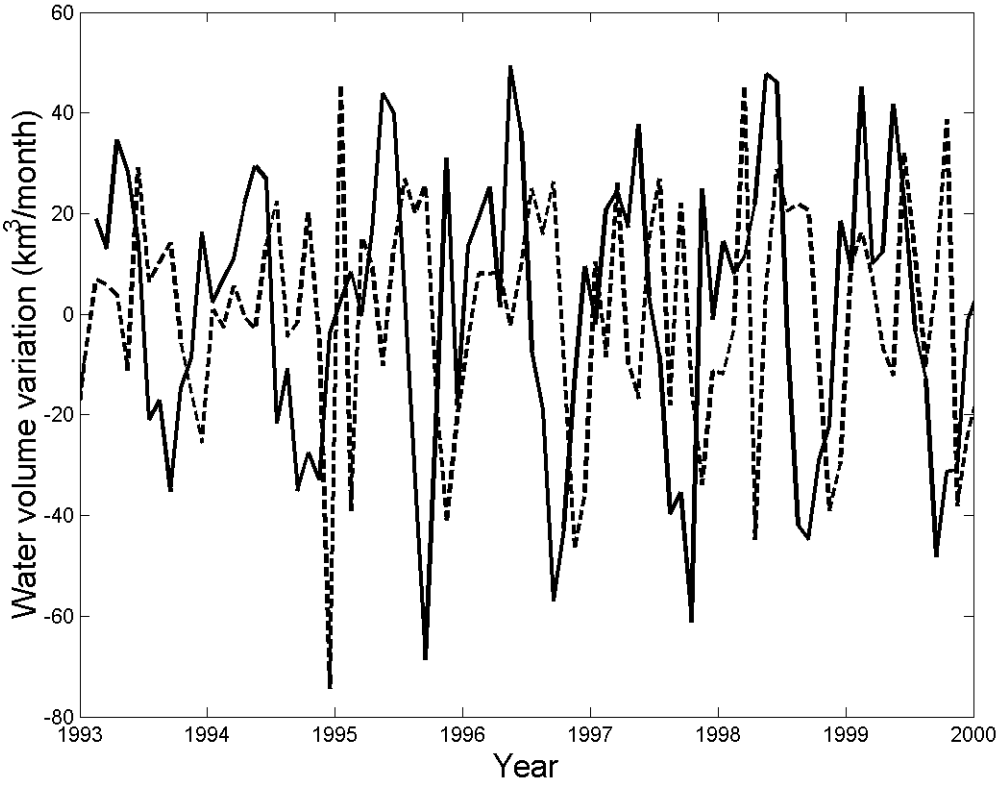
Water volume variation (km3/month)
Year
60
40
20
0
-20
-40
-60
-80
1993
1994
1995
1996
1997
1998
1999
2000

Figure 9:

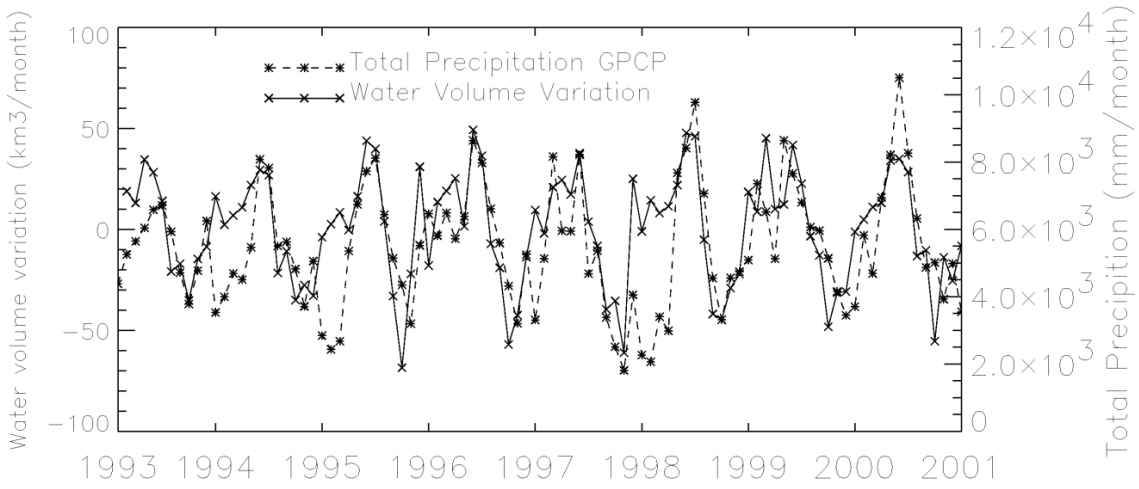
Total Precipitation GPCP
Water Volume Variation
Water volume variation (km3/month)
Total Precipition (mm/month)
100
50
0
−50
−100
1.2×10^4
1.0×10^4
8.0×10^3
6.0×10^3
4.0×10^3
2.0×10^3
0
1993 1994 1995 1996 1997 1998 1999 2000 2001

Figure 10:

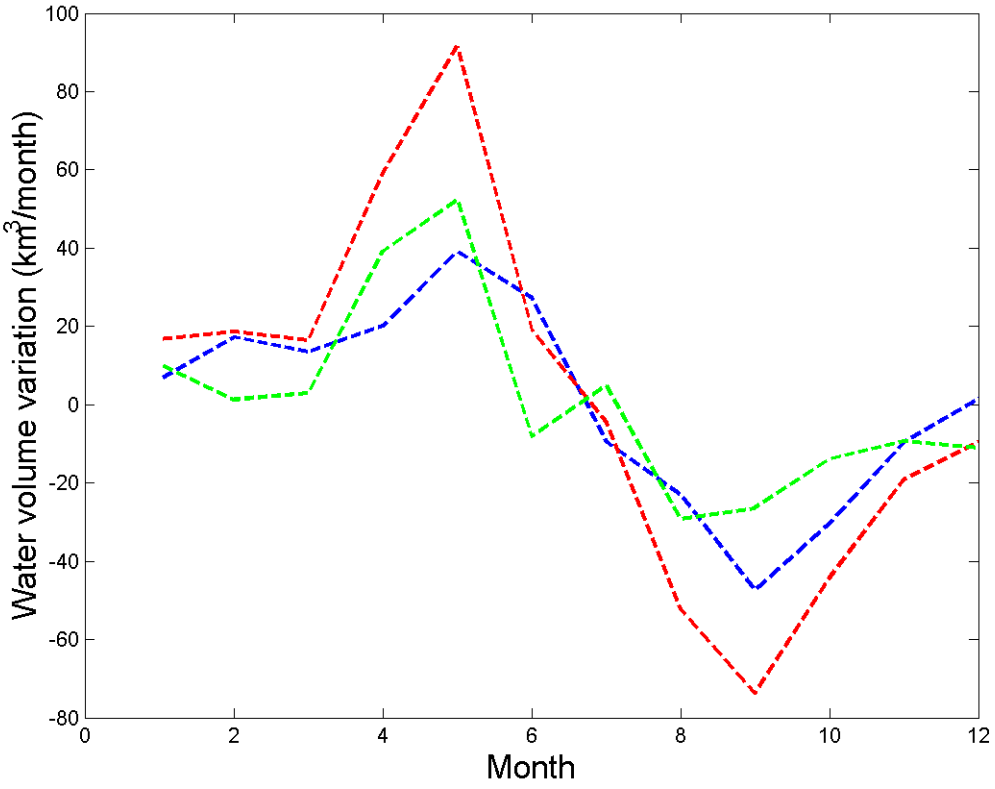
Water volume variation (km3/month)
Month
100
80
60
40
20
0
-20
-40
-60
-80
0
2
4
6
8
10
12